

RESEARCH ARTICLE

Photonic crystal microcrystalline silicon solar cellsYoshinori Tanaka^{1*†}, Kenji Ishizaki^{1†}, Menaka De Zoysa^{1,2†}, Takami Umeda¹,
Yosuke Kawamoto¹, Shoya Fujita¹ and Susumu Noda¹¹ Department of Electronic Science and Engineering, Kyoto University, Kyoto, Japan² The Hakubi Center for Advanced Research, Kyoto University, Kyoto, Japan**ABSTRACT**

Enhancing the absorption of thin-film microcrystalline silicon solar cells over a broadband range in order to improve the energy conversion efficiency is a very important challenge in the development of low cost and stable solar energy harvesting. Here, we demonstrate that a broadband enhancement of the absorption can be achieved by creating a large number of resonant modes associated with two-dimensional photonic crystal band edges. We utilize higher-order optical modes perpendicular to the silicon layer, as well as the band-folding effect by employing photonic crystal superlattice structures. We establish a method to incorporate photonic crystal structures into thin-film (~500 nm) microcrystalline silicon photovoltaic layers while suppressing undesired defects formed in the microcrystalline silicon. The fabricated solar cells exhibit 1.3 times increase of a short circuit current density (from 15.0 mA/cm² to 19.6 mA/cm²) by introducing the photonic crystal structure, and consequently the conversion efficiency increases from 5.6% to 6.8%. Moreover, we theoretically analyze the absorption characteristics in the fabricated cell structure, and reveal that the energy conversion efficiency can be increased beyond 9.5% in a structure less than 1/400 as thick as conventional crystalline silicon solar cells with an efficiency of 24%. © 2015 The Authors. *Progress in Photovoltaics: Research and Applications* published by John Wiley & Sons Ltd.

KEYWORDS

photonic crystal; microcrystalline silicon; solar cell

***Correspondence**

Yoshinori Tanaka, Department of Electronic Science Engineering, Kyoto University, Kyoto, Japan.

E-mail: ytanaka@qoe.kuee.kyoto-u.ac.jp

†These authors contributed equally to this work

This is an open access article under the terms of the Creative Commons Attribution-NonCommercial-NoDerivs License, which permits use and distribution in any medium, provided the original work is properly cited, the use is non-commercial and no modifications or adaptations are made.

Received 2 July 2014; Revised 4 October 2014; Accepted 10 November 2014

1. INTRODUCTION

Interest in renewable energy has continued to increase throughout the world, and consequently, demands on silicon (Si)-based solar cells have been rapidly increasing. Currently, crystalline Si solar cells are commonly used, where the thickness of the photovoltaic layer is about 100–200 μm. Considering the future proliferation of solar cells, the supply of Si resources will become a critical factor. Therefore, the development of thin-film Si solar cells [1–6] is important, where amorphous Si (a-Si) or microcrystalline Si (μc-Si) photovoltaic layers with thicknesses of several hundred nm to several μm are deposited by chemical vapor deposition (CVD). However, the performance of a-Si solar cells is limited by the inherent nature of the material such as a short carrier diffusion length and

light-induced degradation [7]. In contrast, μc-Si is a promising material with no such limitations because the crystalline Si grains in the material provide the main contribution to the photo-current characteristics. However, the optical absorption of μc-Si shows an indirect transition similar to crystalline Si, which lowers the optical absorption within a wavelength range near the crystalline Si electronic band edge, particularly 600–1000 nm. The enhancement of optical absorption in this wavelength region is essential to increase the energy conversion efficiency of solar cells. To overcome this issue, a randomly textured structure [8,9] is widely used, where photons are trapped by scattering effects. However, this randomness implies that the characteristics of each device are different, and undesired defects inside the μc-Si layer degrade the electronic performance. Recently, the application of photonic crystals (PCs) has

been investigated for efficient light absorption in thin layers. Although several reports have predicted the enhancement of light absorption by incorporating PC structures [10–15], the design of such devices is still at the level of parameter adjustment (lattice constant, hole/rod radii, and thickness of PC structures). Definitive guidelines for enhancing optical absorption by PCs have not yet been proposed.

In this work, we establish guidelines for the enhancement of broadband light absorption between 600 and 1000 nm by utilizing multiple large-area resonant modes at the band edge of a PC; higher order modes perpendicular to the Si layer and band-folding effects in photonic superlattice structures are used to create a large number of resonant modes. We use these principles to experimentally demonstrate an increase in light-absorption and energy conversion efficiency. Our method allows the incorporation of PC structures into actual $\mu\text{c-Si}$ solar cells and suppresses the formation of cracks and voids in the $\mu\text{c-Si}$ layer, leading to solar cells that perform better both optically and electrically. The fabricated solar cells exhibit 1.3 times increase of short circuit current density (from 15.0 mA/cm^2 to 19.6 mA/cm^2) by introducing the PC structure, and consequently the conversion efficiency increases from 5.6% to 6.8%. Moreover, theoretical analysis of the Si absorption in the fabricated structure reveals that the expected energy conversion efficiency of our $\mu\text{c-Si}$ solar cells exceeds 9.5% in a structure more than 400 times thinner than conventional crystalline Si solar cells, whose efficiency is 24%.

2. METHODS FOR BROADBAND LIGHT ABSORPTION BY PHOTONIC CRYSTALS

We begin by describing the mechanism of broadband light absorption enhancement in photonic crystals (PC). At the Γ point of a PC, a band-edge resonant mode can be created [16–21]. This resonant mode can be accessed from the normal direction and utilized to trap light in solar cells. A schematic illustration of a solar-cell structure in which such band-edge resonant effects can be applied is shown in Figure 1. The important issue here is to create as many resonant modes as possible in order to trap light over a broad range of wavelengths. Our first strategy is to use the multimode nature of light confined in the vertical direction in $\mu\text{c-Si}$. Figure 2(a) shows a photonic band diagram, assuming a 400-nm-thick Si layer, where the black line corresponds to the fundamental mode and the colored lines correspond to higher-order

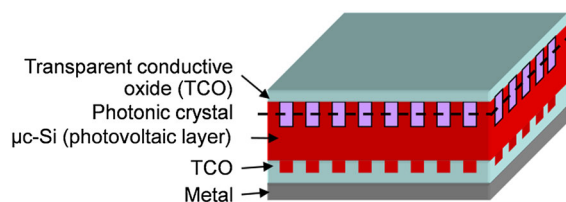


Figure 1. Schematic view of a solar cell with a PC structure.

modes of light confined in the vertical direction. We find that some transverse modes in the vertical direction also appear. These create several resonant modes at the Γ point, whose group velocity is zero. By coupling incident light into these resonant modes, an increase in light absorption at the resonant frequency is expected. Our second strategy is to form a superlattice structure as shown in Figures 2(b) and (c), which provides further band edges at the Γ point due to a reduction in size of the fundamental Brillouin zone.

We have calculated the optical absorption of $\mu\text{c-Si}$ solar cells incorporating the PCs shown in Figure 2 using the three-dimensional (3D) finite difference time domain (FDTD) method. The calculation program is developed by our group, which is based on the Yee's algorithm [22], Berenger's perfectly matched absorbing boundary condition [23], and Bloch's periodic boundary condition. The average thickness of the $\mu\text{c-Si}$ layer was set to 400 nm, and optical absorption in the transparent conductive oxide (TCO) layers was ignored at this stage. The calculated optical absorption spectra for both a 4×4 period superlattice structure and for a solar cell without a PC structure are shown in Figure 3(a), which clearly shows an enhancement in optical absorption using the PC structure. The average optical absorption in the wavelength range from 500 to 1000 nm, weighted by the solar spectrum (AM 1.5) and normalized by the structure without a PC, is shown in Figure 3(b) [21]. Here, in the absorption spectrum of the structure without a PC, we see peaks and dips across the range of calculated wavelengths due to Fabry–Perot interference occurring in the vertical direction. Since such interference both enhances and suppresses the absorption, its influence is negligible when the spectrum is averaged over wavelength. Figure 3(b) shows that introducing a PC significantly enhances the optical absorption, and that a photonic superlattice structure is effective for further enhancement of the optical absorption. We also compared these results with the Lambertian textured structure with the same $\mu\text{c-Si}$ layer thickness. Note that the Lambertian structure, which induces ideal light scattering according to Lambert's cosine law inside the solar-cell structure, is known to indicate the upper limit of the absorption of random-textured solar-cell structure. We found that the absorptivity in these photonic superlattice structures can exceed that of the Lambertian textured structure.

3. GROWTH OF MICROCRYSTALLINE SILICON ON PHOTONIC CRYSTAL STRUCTURES

To demonstrate the mechanism described above, we now discuss how to incorporate PC structures into actual $\mu\text{c-Si}$ solar cells. We investigated the growth of a $\mu\text{c-Si}$ layer on a PC structure using a very-high frequency (VHF) plasma-enhanced chemical vapor deposition (PE-CVD) method. First, a square-lattice cylindrical-rod-type SiO_2 PC was fabricated using electron-beam lithography and reactive-ion etching, and $\mu\text{c-Si}$ was then deposited on this PC structure.

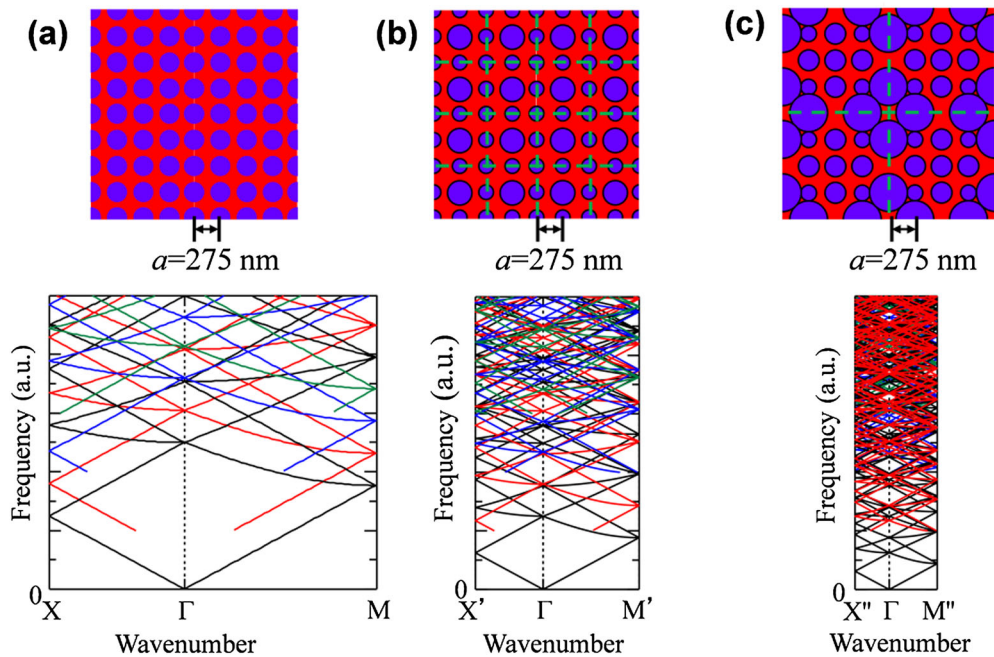


Figure 2. (a) Real space image of the PC structure and photonic band diagram. (b–c) Schematic views of 2×2 and 4×4 period superlattice PCs and their band diagrams.

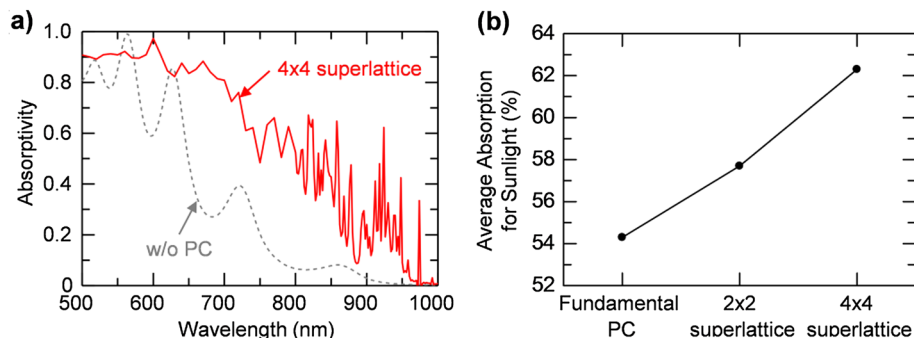


Figure 3. (a) Calculated absorption spectra of solar cells with a 4×4 period superlattice structure and without the PC structure. (b) Average optical absorption in wavelength range 500–1000 nm weighted by the solar spectrum for the structures shown in (b–d) (From ref. 21).

A cross-sectional scanning electron microscope (SEM) image of a sample obtained after the deposition of $\mu\text{-Si}$ is shown in Figure 4(a). It can be seen that voids appear between the SiO_2 rods. It is also apparent that columns of $\mu\text{-Si}$ grown on top of the cylindrical rods meet each other in the upper region of the $\mu\text{-Si}$ layer, where cracks are formed. To suppress the formation of such voids and cracks, we decided to taper the SiO_2 rods by employing an O_2 plasma treatment. The degree of tapering could be controlled by changing the plasma-treatment time. Cross-sectional SEM images of $\mu\text{-Si}$ grown on tapered rods formed by different O_2 plasma treatment times are shown in Figure 4 (b–d). The voids that were previously formed in the $\mu\text{-Si}$ vanished as the rod shape became more tapered. Furthermore, the formation of cracks was also suppressed in $\mu\text{-Si}$ grown on the much smoother tapered rods.

We carried out mid-infrared absorption measurements for a quantitative evaluation of the bonding states at the voids and cracks. Just after the completion of $\mu\text{-Si}$ growth, the surfaces of the voids and cracks are terminated by SiH_x . After the sample has been exposed to the atmosphere for several days, the SiH_x surface termination is oxidized to SiO_x . Therefore, the voids and cracks formed in the $\mu\text{-Si}$ can be characterized by evaluating the concentration of SiO_x bonds. We formed PCs on a ZnO layer instead of a SiO_2 layer in order to eliminate the mid-infrared absorption due to the SiO_2 PC layer. Square-lattice cylindrical-rod-type ZnO PCs were fabricated by electron-beam lithography and reactive-ion etching. The cylindrical rods were tapered using O_2 plasma treatments with different times. Next, $\mu\text{-Si}$ was deposited on these PC structures, and the samples were left in the atmosphere for three days. A

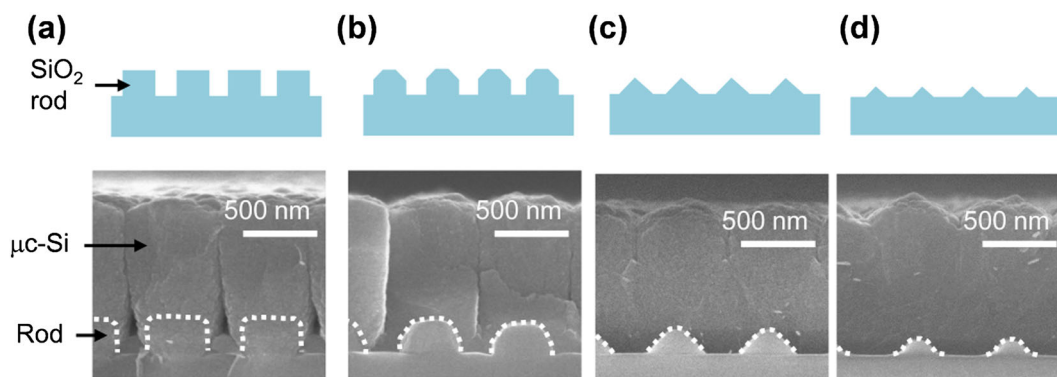


Figure 4. Formation of $\mu\text{c-Si}$ on the rod-type SiO_2 PC with (a) no O_2 plasma treatment; (b–d) O_2 plasma treatment carried out for 18, 42, and 60 min to taper the SiO_2 PC rods.

cross-sectional SEM image of a sample obtained after the growth of the $\mu\text{c-Si}$ layer is shown on the left-hand side of Figure 5. Absorption measurements were carried out using a Fourier transform infrared spectrometer, under the Brewster condition. The results of the transmittance are shown on the right-hand side of Figure 5. A transmission minimum can be seen at a wavenumber of $\sim 2000\text{ cm}^{-1}$, which originates from the SiH_x stretching mode associated with the $\mu\text{c-Si}$ layer. Another minimum is apparent between wavenumbers of $1000\text{--}1200\text{ cm}^{-1}$, which originates from the SiO_x stretching mode [24]. It is clearly seen that the absorption intensity of the SiO_x stretching mode decreases as the PC rods become more tapered. This demonstrates that tapered-rod PCs are essential to suppress oxygen impurity contamination because they eliminate undesired voids and cracks, an important factor in obtaining high-quality films which are essential for high efficiency photoelectric conversion in solar cells.

4. EXPERIMENTAL EVALUATION OF MICROCRYSTALLINE SILICON SOLAR CELLS WITH PHOTONIC CRYSTALS

Based on the results above, we next fabricated $\mu\text{c-Si}$ solar-cell structures. First, we prepared square lattice, tapered-rod-type PC structures on a SiO_2 layer as described above. We then deposited Ag and Ga-doped ZnO (ZnO:Ga) layers as a back reflector and a back electrode using electron-beam evaporation and magnetron sputtering methods, respectively, to entirely cover the SiO_2 PC rod layer. Figure 6(a) shows a top-view scanning electron microscopy (SEM) image of the device after this step. Next, n-doped, intrinsic ($\sim 500\text{ nm}$ thick) and p-doped $\mu\text{c-Si}$ were deposited using PE-CVD. Finally, Sn-doped In_2O_3 (ITO) and mesh-patterned Ag layers were formed by magnetron sputtering and electron beam evaporation. Figure 6(b) shows a cross-sectional SEM image of a fully formed solar cell. We see that the periodic structure was transferred to the top of the device

while the formation of voids and cracks was almost suppressed; interestingly, the top surface has a periodic dome-shaped topology even though the original rods possess a tapered shape. Similar to the case of Figure 4(b), we note that if the $\mu\text{c-Si}$ layer is thicker than the lattice constant, some cracks still exist in the upper part of the $\mu\text{c-Si}$ layer. Therefore, the lattice constant was set at 600 nm for a $\sim 500\text{-nm}$ -thick $\mu\text{c-Si}$ layer. This lattice constant corresponds to the employment of a 2×2 superlattice PC with a fundamental lattice constant of $\sim 300\text{ nm}$, as shown in Figure 2. Therefore, this structure is expected to give rise to multiple band-edge resonant modes and enhanced absorption.

Figure 7(a) shows the measured total absorption spectra for solar-cell structures with and without the PC. An integration sphere was used to measure the total absorption. These results clearly demonstrate that the absorptivity was strongly enhanced by introducing the PC structure, particularly in the wavelength range $600\text{--}1000\text{ nm}$. The presence of many absorption peaks suggests that the enhancement of absorption originates from coupling to multiple band-edge resonance modes. Figure 7(b) shows the current–voltage characteristics of these solar cells for standard solar irradiance (AM1.5), which reveals a clear increase of the short-circuit current density from 15.0 mA/cm^2 to 19.6 mA/cm^2 (an enhancement of about 1.3 times) by introducing the PC structure. To determine the experimental wavelength dependence of the photoelectric conversion characteristics, we also evaluated the external quantum efficiency (EQE) as shown in Figure 7(c). We see that the improvement of EQE in the wavelength range between 600 and 1000 nm contributed the enhancement of short-circuit current density. The characteristics of the fabricated solar cells are summarized in Table I. The increase in short-circuit current density enhances the conversion efficiency from 5.6% to 6.8% . Here, the filling factor (FF) of the cell with PC structure was slightly decreased compared with the case without PC. This might be due to a certain amount of residual cracks/voids (defects), although we have suppressed the formation of them by tapering rods as discussed in Figure 5. Further

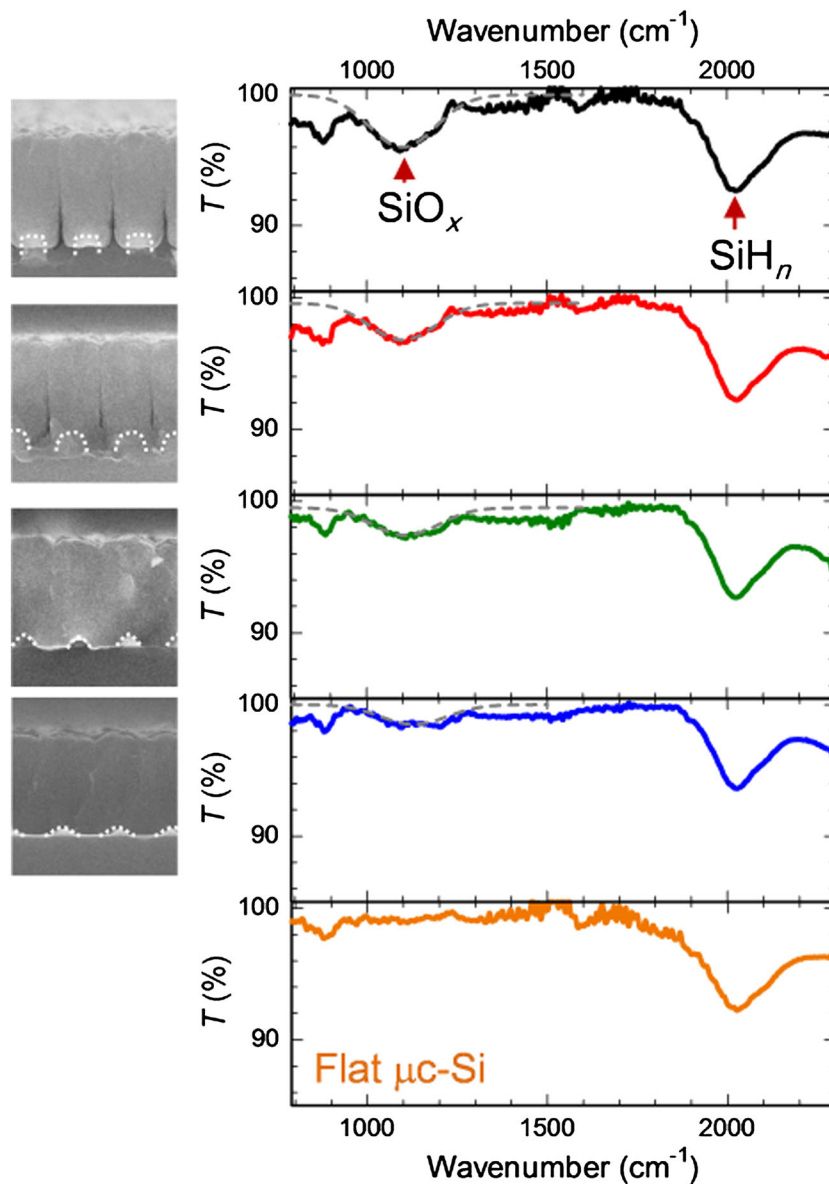


Figure 5. Infrared absorption spectra of $\mu\text{c-Si}$ layers deposited on PC structures with different rod shapes.

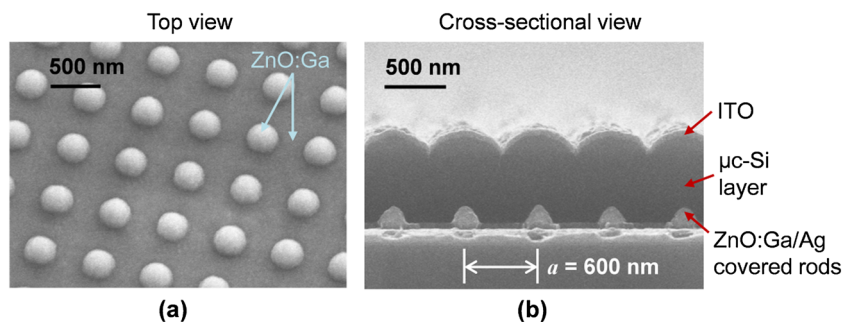


Figure 6. SEM images of the fabricated solar cells incorporating PCs. (a) Top view image after depositing Ag and ZnO:Ga. (b) Cross-sectional image after depositing $\mu\text{c-Si}$ and ITO.

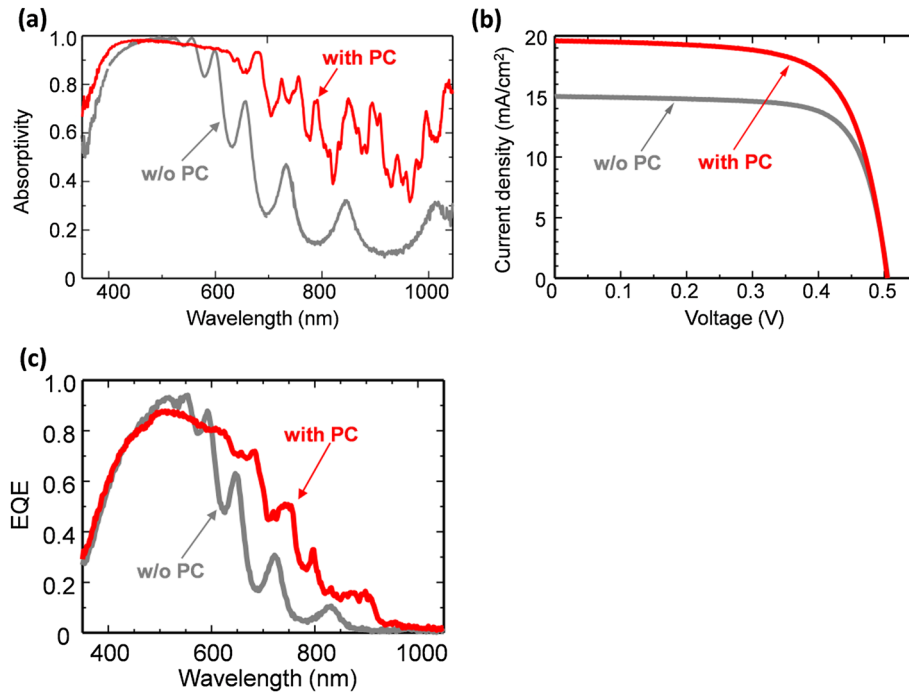


Figure 7. (a) Measured absorption spectra for the full solar-cell structures with and without the PC. (b) Measured current–voltage characteristics of the solar cells, revealing an increase in the short-circuit current density upon incorporation of the PC. (c) Measured external current quantum efficiency (EQE) spectra for the solar-cell structures with and without the PC.

Table I. Summary of the fabricated solar cell's performance.

	J_{sc} (mA/cm ²)	V_{oc} (V)	FF (%)	Efficiency (%)
w/o PC	15.0	0.51	73.3	5.6
with PC	19.6	0.50	69.3	6.8

improvement of rod patterns to reduce defects formed in the $\mu\text{-Si}$ layer can improve the FF as briefly described in the last part of this section.

To investigate the validity of our experimental results, we calculated the optical absorption spectrum of the structure shown in Figure 6 using the 3D FDTD method, which includes tapered rods at the bottom and a periodic dome-shaped top surface. To consider a full cell structure of the fabricated solar cells, we incorporated ITO and ZnO:Ga, including their absorptions, and Ag as a perfect conductor. Calculation results for solar cells without and with the PC structure are shown in Figure 8(a) and (b), respectively. In these figures, the amounts of absorption in each layer are color-coded; the orange area shows a portion absorbed in the $\mu\text{-Si}$ layer, and the green and blue areas show the portions absorbed in ZnO:Ga and ITO, respectively. The white area corresponds to the reflection loss. In the insets shown in Figure 8(b), we calculated the optical absorption distributions in a cross section for several wavelengths. When $\lambda = 804$ nm and 600 nm, most of absorption occurs in the $\mu\text{-Si}$ layer. In contrast, when $\lambda = 1008$ nm, almost all absorption occurs in the top and bottom transparent

conductive oxide (TCO) layers, because the optical absorption of $\mu\text{-Si}$ at this wavelength is much smaller than that of TCO. When $\lambda = 400$ nm, optical absorption occurs in the ITO layer and at the top surface of the $\mu\text{-Si}$ layer due to the large absorption coefficients of both layers.

The total absorption spectrum, which is the sum of the absorptions in all the layers shown in Figures 8(a) and (b), is summarized in Figure 8(c), which reveals an enhancement of the total absorption by the multiple resonant modes as expected when PC is introduced. The calculated spectra of the total absorption agree well with the experimental results shown in Figure 7(a), while the broadening of the experimental absorption peaks might be due to imperfections in the fabricated structure, which are reported to be beneficial for increasing absorption [25,26]. Then, the optical absorptions of only the $\mu\text{-Si}$ layer, which is responsible for the current extraction, are summarized in Figure 8(d) for the cases with and without PCs. It can be seen in Figure 8(d) that EQE is successfully enhanced in the wavelength range between 600 and 1000 nm. However, when we compare the calculation results with the experimental results (Figure 7(c)), the calculation suggests a potential of further improvement of quantum efficiency. From the calculated spectrum of Figure 8(d), we found that short-circuit current density for AM 1.5 would exceed ~ 25 mA/cm² under the assumption of modeling Ag as a perfect conductor, which does not include the plasmonic effect nor absorption. An energy conversion efficiency of more than 9.5% is expected even for a 500-nm-thick

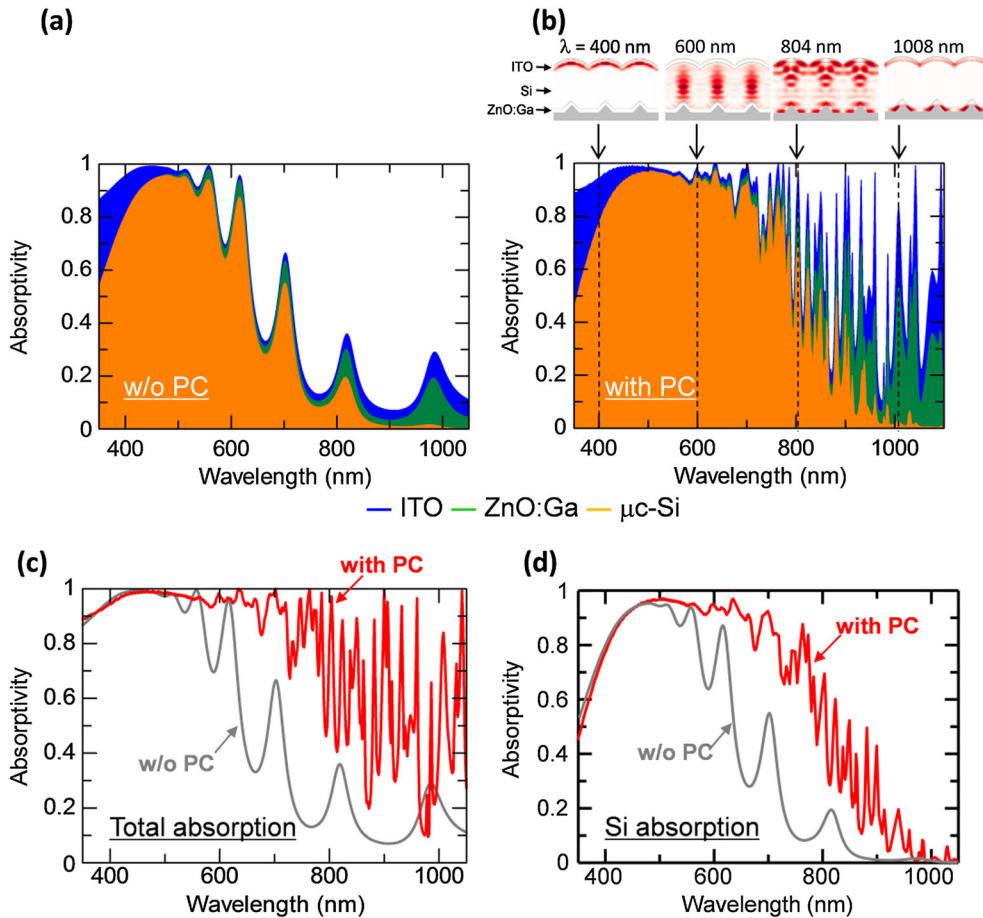


Figure 8. (a),(b) Calculated absorption characteristics for cells without and with the PC, respectively. The insets in (b) show the cross-sectional distribution of absorption at different wavelengths. (c), (d) Spectra of total absorption and absorption of the $\mu\text{c-Si}$.

$\mu\text{c-Si}$ layer, considering the previously reported open circuit voltage of 0.52 V and fill factor of 0.72 [6]. The estimated short-circuit current density exceeds that for Lambertian textured structure with the same $\mu\text{c-Si}$ layer thickness, where we considered losses due to TCO layers in the calculation. This reveals that, although we used a photonic crystal with a lattice constant of 600 nm, which corresponds to a 2×2 superlattice, the realized photonic-crystal solar cell has the potential to increase light absorption comparable to the use of a 4×4 superlattice. This might be due to the effect of a combination of the unique top dome-shaped structure and the bottom rod structure (a detailed analysis will be reported elsewhere). Note that most of the previous reports on $\mu\text{c-Si}$ solar cells have used $\sim 2\text{-}\mu\text{m}$ -thick $\mu\text{c-Si}$ with random textured interfaces and have shown a short-circuit current density of 23–26 mA/cm^2 [2–5,27], whereas our result shows a comparable value, but with much thinner $\mu\text{c-Si}$.

Finally, we discuss the slight decrease of the experimental EQE spectrum (Figure 7(c)) compared to the calculation results (Figure 8(d)). It is possible that some of the carriers generated by light absorption could not be extracted in the real device. To examine this issue, we performed an

electron-beam-induced current (EBIC) measurement over a cross section of the fabricated solar cell, as shown in Figure 9. We used an acceleration voltage of 10 kV to avoid the influence of cut surface states. The top area near the p-doped $\mu\text{c-Si}$ layer responded well compared with the

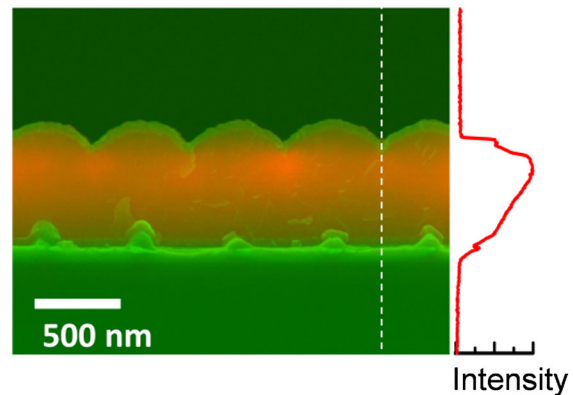


Figure 9. Electron-beam-induced current (EBIC) measurement over a cross section of the fabricated solar cell. The right-hand inset shows a section along the dashed line.

bottom area near the n-doped layer. Because the EBIC response is strong in the area where the built-in electric field is strong, we suggest that an effective depletion layer might only be formed in the top area. We expect that further improvement of the film characteristics of each layer, such as the quality of the intrinsic layer and the doping levels of the p- and n-doped layers, will lead to better experimental cell performances. Indeed, very recently, we have succeeded in increasing J_{sc} , V_{oc} , and FF , and obtained an efficiency of 8.7% (close to ~9.5%). Although the details will be reported elsewhere, claim here is that the adjustment of the crystalline fraction in whole ~500-nm-thick intrinsic μ -Si layer and the appropriate reshaping of the photonic-crystal structure improve the quality of intrinsic μ -Si.

5. CONCLUSION

In summary, we have investigated the enhancement of light absorption and energy conversion efficiency in μ -Si based solar cells by utilizing large-area resonant modes of PCs. We have studied the introduction of PC structures and have developed a method to suppress the formation of defects during the PE-CVD growth of μ -Si. Our fabricated solar cells exhibited an increase of the short-circuit current density from 15.0 mA/cm² to 19.6 mA/cm² (an enhancement of about 1.3 times) when a PC was incorporated; as a result, the conversion efficiency increases from 5.6% to 6.8%. Moreover, our numerical analysis considering the influence of TCO layers has suggested that, if the quality of the μ -Si layer is improved and efficient current extraction from the solar cell to the external circuits is realized, an energy conversion efficiency of more than 9.5% is expected even for a 500-nm-thick μ -Si layer. This would provide a basis to further increase the efficiency of thin-film Si solar cells, including multi-junction solar cells composed of several photovoltaic materials for efficient usage of the broad solar spectrum.

ACKNOWLEDGEMENTS

This work was partly supported by the Core Research for Evolutional Science and Technology (CREST) and the Consortium for Photon Science and Technology (C-PhoST) from the Japan Science and Technology Agency (JST).

REFERENCES

- Vetterl O, Finger F, Carius R, Hapke P, Houben L, Kluth O, Lambert A, Muück A, Rech B, Wagner H. Intrinsic microcrystalline silicon: A new material for photovoltaics. *Solar Energy Materials & Solar Cells* 2000; **62**: 97–108.
- Vetterl O, Lambert A, Dasgupta A, Finger F, Rech B, Kluth O, Wagner H. Thickness dependence of

- microcrystalline silicon solar cell properties. *Solar Energy Materials & Solar Cells* 2001; **66**: 345–351.
- Kondo M. Microcrystalline materials and cells deposited by RF glow discharge. *Solar Energy Materials & Solar Cells* 2003; **78**: 543–566.
- Yamamoto K, Yoshimi M, Tawada Y, Okamoto Y, Nakajima A, Igari S. Thin-film poly-Si solar cells on glass substrate fabricated at low temperature. *Applied Physics A* 1999; **69**: 179–185.
- Sai H, Jia H, Kondo M. Impact of front and rear texture of thin-film microcrystalline silicon solar cells on their light trapping properties. *Applied Physics Letters* 2010; **108**: 044505.
- Sai H, Koida T, Matsui T, Yoshida I, Saito K, Kondo M. Microcrystalline silicon solar cells with 10.5% efficiency realized by improved photon absorption via periodic textures and highly transparent conductive oxide. *Applied Physics Express* 2013; **6**: 104101.
- Staebler DL, Wronski CR. Reversible conductivity changes in discharge produced amorphous Si. *Applied Physics Letters* 1977; **31**: 292–294.
- Yablonovitch E, Cody GD. Intensity enhancement in textured optical sheets for solar cells. *IEEE Transactions on Electron Devices* 1982; **29**: 300–305.
- Sheng X, Johnson SG, Michel J, Kimerling LC. Optimization-based design of surface textures for thin-film Si solar cells. *Optics Express* 2011; **19**: A841–A850.
- Yu Z, Raman A, Fan S. Fundamental limit of nanophotonic light trapping in solar cells. *Proceedings of the National Academy of Sciences* 2010; **107**: 17491–17496.
- Deinega A, Eyderman S, John S. Coupled optical and electrical modeling of solar cell based on conical pore silicon photonic crystals. *Journal of Applied Physics* 2013; **113**: 224501.
- Biswas R, Xu C. Nano-crystalline silicon solar cell architecture with absorption at the classical $4n^2$ limit. *Optics Express* 2011; **19**: A664–A672.
- Wiesendanger S, Zilk M, Pertsch T, Rockstuhl C, Lederer, F. Combining randomly textured surfaces and photonic crystals for the photon management in thin film microcrystalline silicon solar cells. *Optics Express* 2013; **21**: A450–A459.
- Zhu J, Hsu CM, Yu Z, Fan S, Cui Y. Nanodome solar cells with efficient light management and self-cleaning. *Nano Letters* 2010; **10**: 1979–1984.
- Biswas R, Pattnaik S, Xu C, Bhattacharya J, Chakravarty N, Dalal, V. Enhancement of solar cells with photonic and plasmonic crystals – overcoming the Lambertian limit. *Journal of Materials Research* 2013; **28**: 1021–1030.

16. Imada M, Noda S, Chutinan A, Tokuda T, Murata M, Sasaki G. Coherent two-dimensional lasing action in surface-emitting laser with triangular-lattice photonic crystal structure. *Applied Physics Letters* 1999; **75**: 316–318.
17. Miyai E, Sakai K, Okano T, Kunishi W, Ohnishi D, Noda S. Lasers producing tailored beams. *Nature* 2006; **441**: 946–946.
18. Matsubara H, Yoshimoto S, Saito H, Jianglin Y, Tanaka Y, Noda S. GaN photonic-crystal surface emitting laser at blue-violet wavelengths. *Science* 2008; **319**: 445–447.
19. Kitagawa H, Suto T, Fujita M, Tanaka Y, Asano T, Noda S. Green photoluminescence from GaInN photonic crystals. *Applied Physics Express* 2008; **1**: 032004.
20. Zoysa MD, Asano T, Mochizuki K, Oskooi A, Inoue T, Noda S. Conversion of broadband to narrowband thermal emission through energy recycling. *Nature Photonics* 2012; **6**: 535–539.
21. Tanaka Y, Kawamoto Y, Fujita M, Noda S. Enhancement of broadband optical absorption in photovoltaic devices by band-edge effect of photonic crystals. *Optics Express* 2013; **21**: 20111–20118.
22. Yee KS. Numerical solution of initial boundary value problems involving Maxwell's equations in isotropic media. *IEEE Transactions on Antennas and Propagation* 1966; **14**: 302–307.
23. Berenger JP. A perfectly matched layer for the absorption of electromagnetic waves. *Journal of Computer Physics* 1994; **114**: 185–200.
24. Boyd IW, Wilson JIB. A study of thin silicon dioxide films using infrared absorption techniques. *Journal of Applied Physics* 1982; **53**: 4166–4172.
25. Oskooi A, Favuzzi PA, Tanaka Y, Shigeta H, Kawakami Y, Noda S. Partially disordered photonic-crystal thin films for enhanced and robust photovoltaics. *Applied Physics Letters* 2012; **100**: 181110.
26. Oskooi A, Zoysa MD, Ishizaki K, Noda S. Experimental Demonstration of Quasi-resonant Absorption in Silicon Thin Films for Enhanced Solar Light Trapping. *ACS Photonics* 2014; **1**: 304–309.
27. Hänni S, Bugnon G, Parascandolo G, Boccard M, Escarré J, Despeisse M, Meillaud F, Ballif C. High-efficiency microcrystalline silicon single-junction solar cells. *Progress in Photovoltaics: Research and Applications* 2013; **21**: 821–826.